PVP Incorporation Effects on the Structural, Thermal, Electrical, and Mechanical Properties of PVDF-HFP/PVP Blend

Pratiksha Gami, Manish Badole, Asish Kumar Das, Hari Narayanan Vasavan, Samriddhi Saxena, Neha Dagar, and Sunil Kumar*

Department of Metallurgical Engineering and Materials Science, Indian Institute of Technology Indore, Simrol, 453552, India.

*Corresponding author, E-mail: sunil@iiti.ac.in

Abstract

Flexible free-standing membranes (thickness ~ 60 μm) of poly (vinylidene fluoride-co-hexafluoropropylene)/polyvinyl pyrrolidone (PVDF-HFP/PVP) blends with various weight fractions of PVP were fabricated by the solution casting technique. The inclusion of PVP enhanced the semi-crystalline polymer PVDF-HFP's amorphous region, as confirmed by X-ray diffraction (XRD). Fourier transform infrared microscopy (FT-IR) investigations of the macromolecular blend membranes revealed interactions between the PVP and PVDF-HFP. The impact of adding PVP to PVDF-HFP on the miscibility of the resulting blends was examined using scanning electron microscopy (SEM). The results of thermogravimetric analysis (TGA) and differential scanning calorimetry (DSC) confirmed a complete miscibility of PVDF-HFP with PVP. Additionally, the Coats-Redfern model was used to calculate the activation energies of all samples. The uniform dispersion of PVP significantly boosted the thermal stability of the PVDF-HFP-based blend. The PVDF-HFP: PVP (75:25) blend polymer showed the minimum electrical conductivity (σ_{DC}) of ~ 1.23×10^{-14} S cm^{-1}. Adding PVP to the polymer causes additional relaxation because of the PVP/PVDF-HFP interface, which increases the blend's dielectric constant ε_r to 9.6 for the sample with 25% PVP. Dynamic mechanical analysis (DMA) showed an improvement in the storage modulus of blended polymer, with the 25% PVP sample exhibiting a storage modulus of ~0.23 GPa at ~45 °C. These advantageous improvements suggest that the PVDF-HFP/PVP blend is well-suited for insulating applications.

Keywords: Polymer blend, Miscibility, Thermal properties, Conductivity, Dielectric relaxation

1. Introduction

Developing polymer blends has emerged as a critical strategy in pursuing advanced materials with tailored properties [1, 2]. Macromolecular blends encompassing crystalline Poly (vinylidene fluoride-co-hexafluoropropylene) have demonstrated outstanding potential in several electronic applications, including sensor systems, energy storage devices, and high-performance membranes [3-7]. This is evidenced by its exceptional electroactive qualities, including ferroelectricity and piezoelectricity, and its excellent thermal stability (up to 150 °C) [8-10]. Its mechanical malleability and durability make it useful in various applications, including filtration membranes and separator & polymer electrolytes for energy storage applications [11, 12]. The semi-crystalline structure of PVDF-HFP is shaped by factors such as preparation conditions, solvent choices, and the use of additives, which impact its crystallinity and phase composition, including the α, β, γ, δ, and ε phases [13-16]. Generally, the α-phase, which is non-polar, is the dominant form, particularly when the polymer is melt-crystallized at temperatures below 160 °C [17]. However, the β-phase, which is more polar, can be promoted through mechanical deformation or by incorporating various fillers, such as inorganic ceramic particles or clay minerals [18, 19]. It has been demonstrated in earlier studies that adding amorphous, hydrophilic polyvinyl pyrrolidone can encourage PVDF-HFP to form the polar β-phase [20].

Water-soluble nature, biocompatibility, film-forming properties, and capacity to produce transparent, self-standing films are all credited with the usefulness of PVP polymer [21, 22]. It is an essential ingredient in many cosmetics, medicines, and industrial applications due to its solubility in water and organic solvents [23-25]. PVP interacts well with other polymers and reagents due to its weak basicity and capacity to form hydrogen bonds [26]. For example, a blend of PVP with polyvinyl alcohol (PVA) demonstrated a viable matrix for hosting assisted transport carriers to enhance CO_2 permeance [27]. Additionally, the PVDF-HFP/PVP blend incorporates MoO_3 nanowires with the ability to form coating films on wood [28]. Similarly, the Ag@PVP/PVDF nanocomposite, which included silver core-shell nanoparticles covered with PVP for improved dispersion, showed low dielectric loss and high permittivity [29]. PVDF-HFP/PVP blend leverages the strengths of both polymers, resulting in a material with enhanced properties [30]. A common characteristic of PVDF-HFP/PVP blends is that PVP has a glass transition temperature of around 160 °C, comparable to the melting temperatures of PVDF-HFP at about 145 °C. This implies that PVP may be examined during the crystallization process of PVDF-HFP while in a glass state. The blend's improved solubility, flexibility, and mechanical strength make it suitable for various advanced applications, including electronic devices, medical implants, and protective coatings [31-33].

This work involves the incorporation of PVP into PVDF-HFP using the solution casting technique. The structural characterizations were done using X-ray diffraction (XRD), Fourier-transformed infrared spectroscopy (FT-IR), and scanning electron microscope (SEM). The miscibility was further investigated using Thermogravimetric analysis (TGA) and differential scanning calorimetry (DSC). The dielectric constant and storage modulus were measured to quantify the mechanical and electrical characteristics.

2. Experimental Method

2.1. Materials

Prior to use, PVP (average M_W = 360 k from Loba Chemie, India) and P(VDF-HFP) (average M_W = 400 k from Sigma-Aldrich, USA) were vacuum-dried for 5 h at 100 °C. Dimethyl formamide (DMF) was bought from SRL, India. DMF solvent was used exactly as supplied.

2.2 Film Fabrication

Using the conventional solution casting approach, blend polymer membranes of PVDF-HFP with the PVP loadings of 10, 20, 25, 30, and 40 wt.% were fabricated. Further, this will be denoted as DVP*x* (where *x* = 10, 20, 25, 30 and 40 wt.%). We dissolved PVDF-HFP and PVP in 4 ml of DMF. The consequent macromolecular solution was stirred constantly for 12 h at room temperature (RT) to prepare a homogenous blend. To remove DMF, the as-prepared slurries were poured into Teflon Petri dishes and left to evaporate at RT for a whole night. After that, DVP*x* membranes were placed in a vacuum oven at 70 °C for 24 h to remove any traces of DMF. The free-standing membranes that were obtained had thicknesses of ~60 μm. Then, it was punched into discs of 16 mm diameter and stored in an Ar-filled glove box to prevent these from moisture exposure before further characterization.

2.3. Characterizations

An Empyrean - Malvern Panalytical diffractometer was used to acquire as-prepared films' X-ray diffraction patterns (2θ range: 10°–60°). The samples' morphology and surface microstructures were determined using a JEOL-7610+ field-emission scanning electron microscope (FESEM). The samples were first sputter-coated with gold to minimize charging during SEM imaging. PerkinElmer Spectrum IR (Spectrum Two) equipment was utilized to record the FTIR spectrum analysis of a solid polymer membrane in a range of 4000 - 400 cm^{-1}. Using a DSC POLYMA 214 (Netsch) differential scanning calorimeter, the temperature-dependent phase transition properties of the DVP*x* membranes were examined. DVP*x* samples for the DSC were put in aluminum pans and scanned at a rate of 10 °C min^{-1} from -50 to 300 °C. The thermal stability of the as-prepared membranes was measured using thermogravimetric analysis with a PerkinElmer Simultaneous Thermal Analyzer (model number: STA 8000). The measurements were conducted over 30 to 400 °C at a 10 °C min^{-1} heating rate. The current-voltage (I-V) characteristic measurement was used to ascertain the DC conduction of the films at room temperature (Keithley Source Meter Unit 2450-EC). The frequency-dependent dielectric responses at RT were measured using an LCR meter (NF corp. ZM2376). The PerkinElmer **(**DMA-8000) was used to perform dynamic mechanical analysis, which examined the temperature-dependent segmental dynamics of polymer molecules.

3. Results and discussion

3.1. Structural Characterizations

The XRD study was used to examine the amorphous nature of synthesized DVP*x* samples. XRD patterns of PVDF-HFP with varying wt.% of PVP polymer blends are displayed in Fig. 1. A prominent broad peak was observed around 2θ ~20° [34]. As PVP content increased, the splitting of (100) and (020) peaks became lesser due to the broadening of peaks which could be attributed to the reduction in average crystallite size of the PVDF-HFP [30, 35]. This confirms the increased proportion of amorphous regions in the polymer blend (Fig. 1(f-g)).

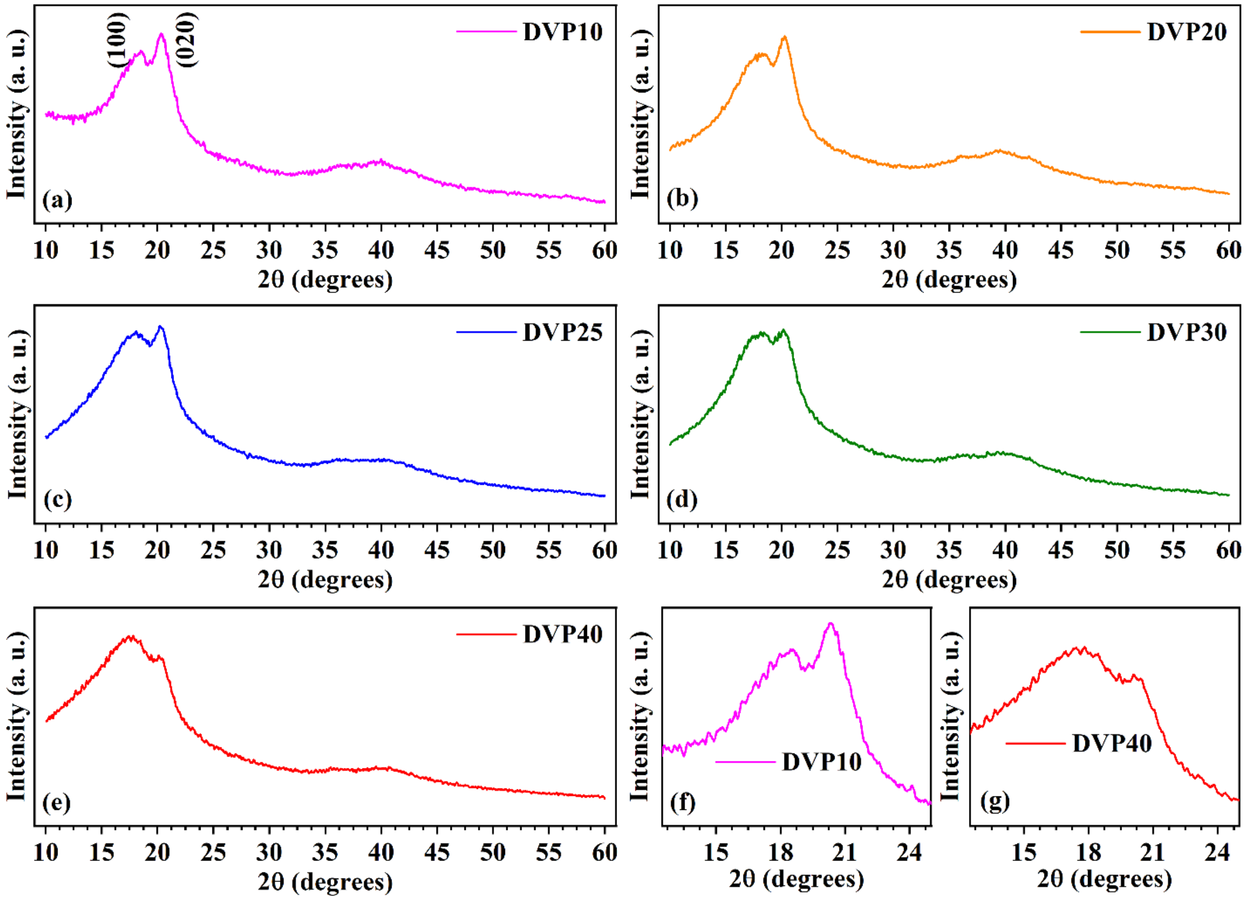

Fig. 1. XRD patterns of (a) DVP10, (b) DVP20, (c) DVP25, (d) DVP30, and (e) DVP40 membranes. To illustrate the peak broadening in the range from 12.5 °- 25°, the magnified views are displayed in (f) DVP10 and (g) DVP40.

Fourier-transformed infrared spectroscopy (FT-IR) analysis was performed to acquire interactions among molecules in DVP*x* at RT. Adding PVP to the polymer matrix of PVDF-HFP affects the vibrational modes, resulting in variations in peak intensities and shifting within the spectra. The FT-IR spectra for the PVDF-HFP/PVP films with various PVP wt.% are shown in Fig. 2. The peaks shifting at 2930 cm^{-1} and 1176 cm^{-1}, belong to CH_2 asymmetrical stretching and C-F asymmetric stretching, respectively [36]. A peak at 1298 cm^{-1} is responsible for the C-N stretching of the aromatic amine of PVP, which becomes more pronounced as the PVP concentration increases [37, 38]. A band at 1390 cm^{-1} confirms CH_2 wagging within the DVP*x* blend polymers [39]. The FT-IR bands at 880 cm^{-1} indicate the presence of the γ-phase in the PVDF-HFP [40].

The mixed modes of molecular vibrations at 840 cm^{-1} indicate the β-phase of PVDF-HFP, CH$_2$-rocking, and -CF$_2$- stretching [41]. The transmittance peak at 1676 cm^{-1} was present due to some intermolecular H-bonding or dipole-dipole interactions between the intermolecular carbonyl of PVP entities [38]. A peak at 735 cm^{-1} indicates a C-H wagging vibration of the imidazolium ring in PVP. The peak corresponding to 658 cm^{-1} and 576 cm^{-1} is related to C-H vibrations.

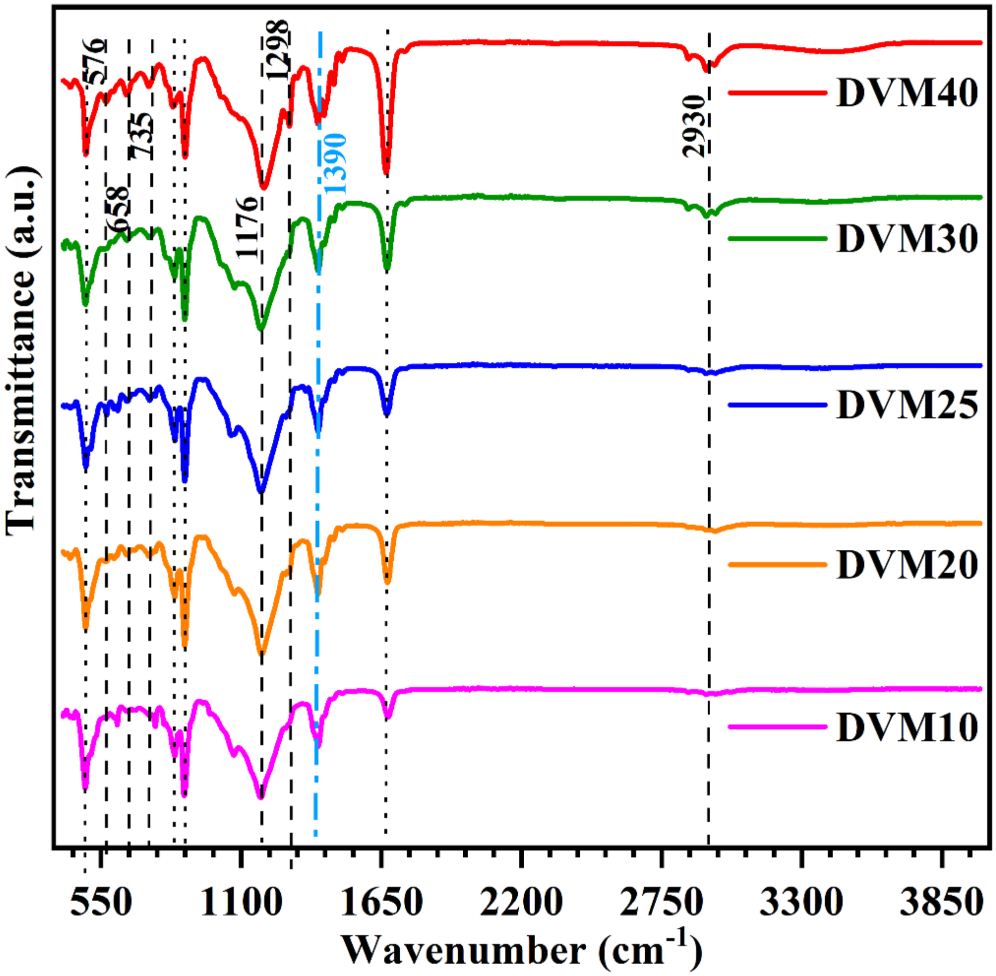

Fig. 2. FT-IR spectra of DVPx (x = 10, 20, 25, 30, and 40) films. The light blue dash-dot line indicates that CH$_2$ wagging is confirmed in the DVPx blend polymers.

The morphological and microstructural characteristics of the as-prepared blends were investigated using SEM analysis (Fig. 3). Figure 3(a-d)) shows that smooth surfaces were found up to DVP30, indicating the complete miscibility of the polymer blend. The segregated PVP polymer was noticed in the DVP40 film, signifying a phase separation or partial miscibility of the resultant blend, as reflected in Fig. 3(e) [30].

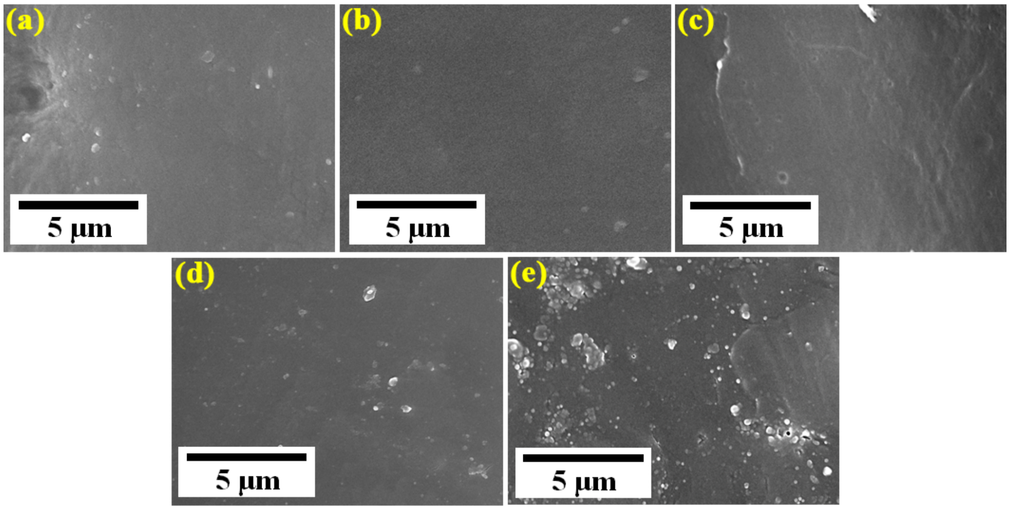

Fig. 3. SEM micrographs of (a) DVP10, (b) DVP20, (c) DVP25, (d) DVP30, and (e) DVP40 membranes.

3.2. Thermal Characterizations

TGA was used to investigate the thermal characteristics of macromolecules by examining the effects of applied temperature (30 °C to 680 °C under N_2 environment) on the material's residual weight (Fig. 4(a)). The thermograms are composed of two significant phases of deterioration, first at 70 - 110 °C representing removing absorbed moisture. The second stage (280 - 490 °C) indicates that the most stable organic backbone or pendant functional groups inside the polymeric scaffold were pyrolyzed. The impact of PVP on the PVDF-HFP thermal decomposition rate was modeled using the Coats-Redfern model [42, 43]. The model, depending on the residual mass, is a valuable technique for calculating activation energy (E_a) for thermal degradation using the following relation:

$$\log\left[\frac{-\log\,(1-\alpha)}{T^2}\right] = \log\frac{R}{E_a}\left[\frac{E_a-2RT}{E_a}\right] - 0.434\,\frac{E_a}{RT} \qquad (1)$$

Here, T represents the absolute temperature (K), R is the gas constant (8.314 J mol^{-1} K^{-1}), and α refers to the fractional weight loss at a particular temperature. The activation energy of each membrane was calculated by plotting log (-log (1 - α)/T^2) *vs.* (1000/T) and fitting straight lines to yield slopes (-E_a/2.303R). The resulting E_a of each membrane is given in Table 1. This table shows that the activation energies for the blends were higher with increasing PVP content up to DVP25. However, beyond this point, the activation energies decreased as the PVP content increased. This finding suggests that the existing blend is appropriate for various possible uses.

Table 1. The activation energy calculated using the Coats-Redfern model, the decomposition temperature at 50% weight loss (T_{50}), melting temperature (T_m), enthalpy of fusion (ΔH_c), and degree of crystallinity (Xc) for all DVPx samples.

Sample	**E_a (kJ mol^{-1})**	**T_{50} (°C)**	**T_m (°C)**	**ΔH_c (J g^{-1})**	***Xc (%)***
DVP10	26.88	438	94	85.06	73.60
DVP20	27.22	456	85	61.55	47.34
DVP25	28.29	464	72	50.27	36.25
DVP30	28.08	458	78	58.58	39.43
DVP40	27.85	445	90	76.14	43.92

Figure 4(b) shows the DSC thermograms of the polymer blends. The samples were heated at 10 °C min^{-1} within the specified temperature range (30 – 680 °C). Table 1 presents the melting point (T_m) of the as-prepared films. The blue highlighted area of Fig. 4(b) depicts the glass transition temperature range (-44.4 °C to -43.4 °C) for all DVP*x*, which is lower than PVP (~160 °C) [44]. Adding polyvinyl pyrrolidone to PVDF-HFP initially lowers the glass transition temperature (Tg), but enhanced secondary interactions between the polymers increase Tg for higher PVP content samples (DVP30 and DVP40). A quantitative estimation of the percentage of crystallinity (Xc) of the membranes was derived from the DSC data (Table 1). This can be calculated using the following equation:

$$\text{Crystallinity } (Xc) = \frac{\Delta H_c}{(1-x)\,\Delta H_m^0} \times 100 \tag{2}$$

where ΔH_c is the enthalpy of fusion obtained from the melting peak area, ΔH_m^0 is the melting enthalpy of 100% crystalline PVDF-HFP (104 J g^{-1}), and x is the PVP weight fraction. Since PVP is an amorphous polymer, it does not contribute to crystallinity in the blend. Therefore, the crystallinity calculation is based solely on the PVDF-HFP fraction.

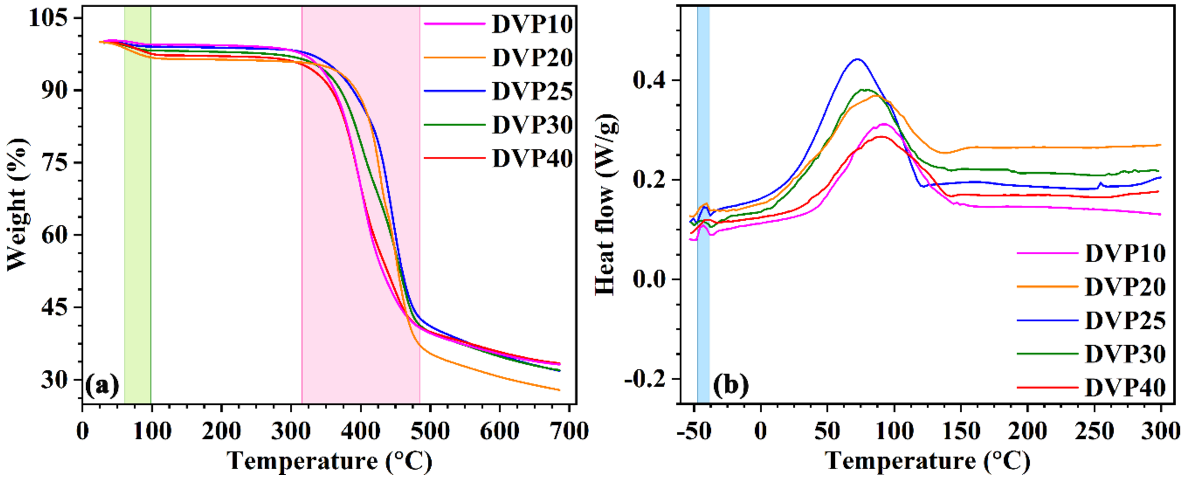

Fig. 4. (a) TGA and (b) DSC thermograms of DVPx (x = 10, 20, 25, 30, 35, and 40) membranes at a heating rate of 10 °C min^{-1}.

3.3. Electrical Properties

The I–V characteristics of each sample in the voltage range of -5 V to +5 V at RT are displayed in Fig. 5. The DC conductivity values for the as-prepared films were obtained by linearly fitting the current-voltage curve at RT (Table 2). The room temperature DC conduction decreased with the addition of PVP up to 25 wt.%, then increased with DVP30 and DVP40. Many dielectric polymers are known for their electrically insulating properties because of their intricate molecular structures and covalent bonds, preventing electrons from moving long distances [45]. Here, DVP25's lowest electronic conductivity indicates that the polymer blend is excellent for use as an insulator in relevant applications.

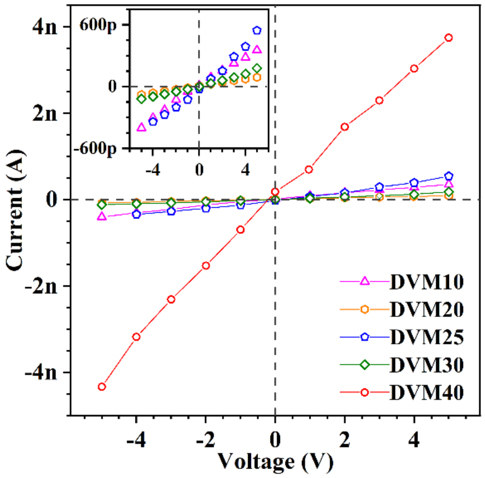

Fig. 5. I-V characteristics of DVPx (x = 10, 20, 25, 30, and 40) membranes at RT.

To investigate the dielectric characteristics of DVP*x* polymer blend films, the dielectric constant (ε_r) and dielectric loss (tanδ) were measured at room temperature in the frequency range of 10^2 - 10^6 Hz (Fig. 6). The dielectric constant first increased from 6.6 (at 1 MHz) for DVP10 to 9.5 for 25% PVP sample. Then, it decreased with further PVP incorporation in PVDF-HFP (Fig 6(a)) [46]. A high value of ε_r at low-frequency region in all samples was noticed. The highest dielectric constant (at 1 MHz) was obtained, ~9.6 for DVP25 polymer blend films, which is 1.14 times greater than pure PVDF-HFP (~8.4) [47]. This could be attributed to the high interfacial polarization at the PVP/PVDF-HFP interface in the DVP25 polymer film. According to the Maxwell-Wagner effect, charges accumulate at the PVP/PVDF-HFP interface due to the variations in conductivity (PVP has higher electron mobility than PVDF-HFP) between the multiphase of polymer blends and cause interfacial polarization [48, 49]. Nevertheless, segregation occurred as the PVP content increased, which lowered the internal effective interface area between the PVP particles and the PVDF-HFP matrix, thereby suppressing the interfacial polarization [50, 51]. Thus, a decrement in the dielectric constant values of the DVP30 and DVP40 polymer blends was observed [52].

Table 2: Room temperature DC conductivity (σ_{DC}) and dielectric constant (ε_r) for DVPx membranes.

Sample	σ_{DC} **(S cm^{-1}) (RT)**	ε_r **(@1 MHz)**
DVP10	3.46×10^{-13}	6.6
DVP20	3.24×10^{-14}	8.3
DVP25	1.23×10^{-14}	9.5
DVP30	9.94×10^{-14}	8.9
DVP40	3.56×10^{-12}	7.3

Figure 6(b) represents the tanδ vs. frequency plot for all the prepared films. The observed values of tanδ for all the samples were ~ 0.07 at 1 MHz, which suggests the low loss behavior of polymer blends. The high value of tanδ in low frequencies region was noticed, which is attributed to the sample-electrode interface polarization (space charge polarization) as displayed in Fig 6(b).

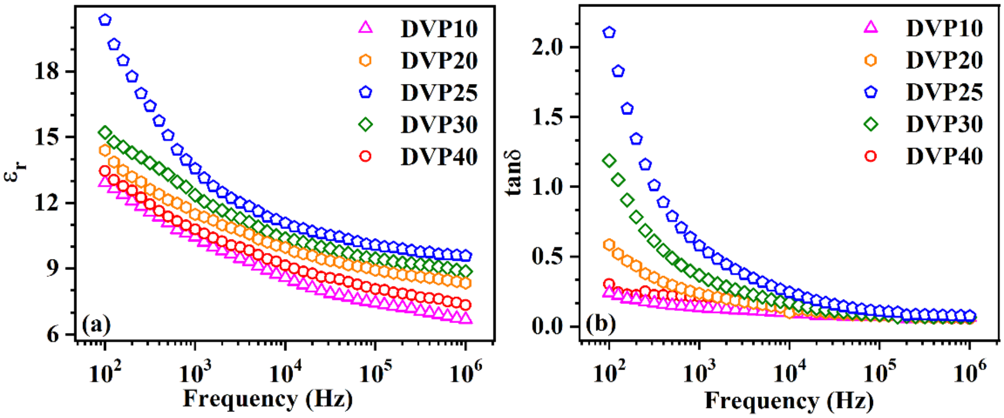

Fig. 6(a) Dielectric constant (ε_r) and (b) tanδ with a frequency range from 10^2 – 10^6 Hz for all DVPx (x = 10, 20, 25, 30, 35 and 40) polymer blend films.

3.4. Mechanical properties

The viscoelastic characteristics of the polymer-polymer composites were assessed using dynamic mechanical analysis (DMA), emphasizing the storage modulus and loss factor. The DMA curves for the composites with the labels DVP10, DVP25, and DVP40 are shown in Fig. 7. The storage modulus and tanδ_M curves for the DVP10 sample show a peak at about 70 °C, suggesting a significant change in its mechanical characteristics at this temperature. DVP40 has the highest storage modulus of all the films, measuring 0.34 Gpa (at ~40 °C), indicating that it is more rigid than the others [53]. However, this value is still significantly lower than the storage modulus of pure PVDF-HFP (~1.6 Gpa) [30]. Its loss factor is ~0.42 at 80 °C, which is higher than that of DVP10 and DVP25. PVP limits the mobility of the polymer chains in the polymer matrix, which affects the material's characteristics [54]. This constraint impacts the composite's relaxing behavior. PVP specifically causes a decrease in molecular mobility, which causes the relaxation process to proceed in the composite samples at a lower temperature than in pure polymers [55]. The observed variations in storage modulus and loss factor are the consequence of this shift.

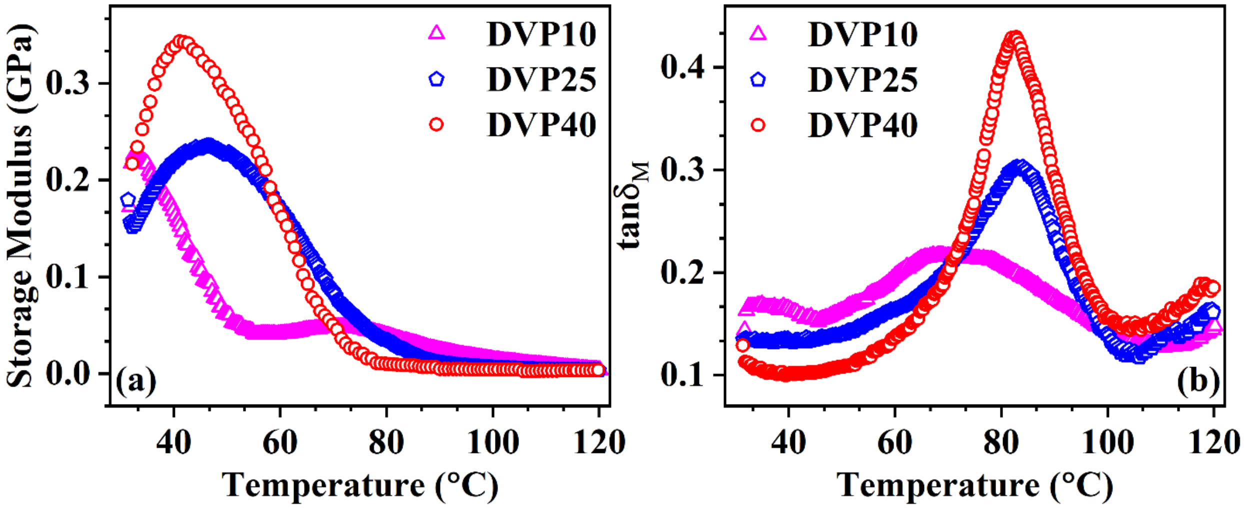

Fig. 7. The DMA curves (a) storage modulus vs. frequency and (b) tanδ_M vs. frequency for DVPx (x = 10, 25, and 40) polymer blend membranes.

4. Conclusions

In conclusion, the PVDF-HFP/PVP blends were fabricated via solution casting. XRD analysis indicates that increasing the PVP content affects the crystallinity of the PVDF-HFP polymer. FT-IR spectroscopy confirms the interaction between PVDF-HFP and PVP, highlighted by the light blue color of FT-IR peaks at ~1390 cm^{-1}. SEM micrograph confirmed a smooth surface for DVP25. Further, TGA and DSC analyses confirm the complete miscibility of the PVDF-HFP and PVP films, as evidenced by observing a single glass transition temperature and melting point. I-V measurement demonstrates that DVP25 exhibits the lowest DC electrical conductivity of 1.2×10^{-14} S cm^{-1}, suggesting the insulating nature of the blend. The highest value of dielectric constant (~ 9.6) of DVP25 indicates that the addition of PVP enhances interfacial polarization. However, excessive PVP content reduces the effective surface area between PVP and PVDF-HFP, decreasing the dielectric constant for DVP30 and DVP40. Dynamic mechanical analysis reveals that incorporating PVP lowers the blends' storage modulus compared to pure PVDF-HFP, suggesting a decrease in mechanical rigidity. This work demonstrates PVP's beneficial effects on the dielectric and mechanical properties of PVDF-HFP polymer, and DVP25 could be a potential candidate for relevant insulating applications.

Declaration of competing interest

The authors declare that they have no known competing financial interests or personal relationships that could have appeared to influence the work reported in this paper.

Acknowledgments

SK thanks the Science and Engineering Research Board (SERB) for the Core Research Grant (Grant no. CRG/2021/005548). The Ministry of Education is also gratefully acknowledged for funding (Grant no. MoE-STARS/STARS-2/2023-0365).

Data availability

Data will be made available on request.

References

[1] L. Zhao, X. Peng, X. Liu, Y. Wang, S. Qin, J. Zhang, Miscibility and morphology of binary crystalline blends of poly(L-lactide) and poly(butylene adipate), Polym. J. 45(9) (2013) 929-937 10.1038/pj.2013.10.

[2] J. Parameswaranpillai, S. Thomas, Y. Grohens, Polymer Blends: State of the Art, New Challenges, and Opportunities, Characterization of Polymer Blends2014, pp. 1-6.

[3] R.R. Karthieka, T. Prakash, Dose-dependent X-ray sensing behaviour of $Cs_3Bi_2I_9$: PVDF-HFP nanocomposites, Physica E Low Dimens. Syst. Nanostruct. 133 (2021) 114823 10.1016/j.physe.2021.114823.

[4] A. Daneshkhah, S. Shrestha, M. Agarwal, K. Varahramyan, Poly(vinylidene fluoride-hexafluoropropylene) composite sensors for volatile organic compounds detection in breath, Sens. Actuators B Chem. 221 (2015) 635-643 10.1016/j.snb.2015.06.145.

[5] A.K. Das, M. Badole, H.N. Vasavan, S. Saxena, P. Gami, S. Kumar, Highly conductive ceramic-in-polymer composite electrolyte enabling superior electrochemical performance for all-solid-state lithium batteries, Ceram. Int. 49(18) (2023) 29719-29728 10.1016/j.ceramint.2023.06.214.

[6] N. Terasawa, N. Ono, Y. Hayakawa, K. Mukai, T. Koga, N. Higashi, K. Asaka, Effect of hexafluoropropylene on the performance of poly(vinylidene fluoride) polymer actuators based on single-walled carbon nanotube–ionic liquid gel, Sens. Actuators B Chem. 160(1) (2011) 161-167 10.1016/j.snb.2011.07.027.

[7] P. Gami, M. Badole, H.N. Vasavan, A.K. Das, S. Saxena, S. Kumar, Y-Doped $LiZr_2(PO_4)_3$ in a PVDF-HFP Composite Electrolyte for Solid-State Li-Metal Batteries, ACS Appl. Energy Mater. 2(5) (2024) 1278-1287 10.1021/acsaenm.4c00076.

[8] J. Chen, J. Fan, M. Livojevic, M. Gupta, T. Tang, C. Ayranci, Enhancing piezoelectric properties of PVDF-HFP composite nanofibers with cellulose nanocrystals, Mater. Today Commun. 39 (2024) 108872 10.1016/j.mtcomm.2024.108872.

[9] X. He, K. Yao, B.K. Gan, Phase transition and properties of a ferroelectric poly(vinylidene fluoride-hexafluoropropylene) copolymer, J. Appl. Phys. 97(8) (2005) 10.1063/1.1862323.

[10] J.-H. Cao, B.-K. Zhu, Y.-Y. Xu, Structure and ionic conductivity of porous polymer electrolytes based on PVDF-HFP copolymer membranes, J. Membr. Sci. 281(1) (2006) 446-453 10.1016/j.memsci.2006.04.013.

[11] A.K. Das, M. Badole, H.N. Vasavan, S. Saxena, P. Gami, N. Dagar, S. Kumar, $LiTa_2PO_8$-Based Polymer–Ceramic Electrolyte Paved the Way to High-Performance Solid-State Lithium Metal Batteries, ENERG FUEL 38(12) (2024) 11253-11261 10.1021/acs.energyfuels.4c01520.

[12] D. Zhou, D. Shanmukaraj, A. Tkacheva, M. Armand, G. Wang, Polymer Electrolytes for Lithium-Based Batteries: Advances and Prospects, Chem 5(9) (2019) 2326-2352 10.1016/j.chempr.2019.05.009.

[13] Z. Jin, D. Lei, Y. Wang, L. Wu, N. Hu, Influences of poling temperature and elongation ratio on PVDF-HFP piezoelectric films, Nanotechnol. Rev. 10 (2021) 1009-1017 10.1515/ntrev-2021-0070.

[14] D. Lei, N. Hu, L. Wu, R. Huang, A. Lee, Z. Jin, Y. Wang, Preparation of efficient piezoelectric PVDF–HFP/Ni composite films by high electric field poling, 11(1) (2022) 452-462 doi:10.1515/ntrev-2022-0025.

[15] B. Luo, X. Wang, H. Wang, Z. Cai, L. Li, P(VDF-HFP)/PMMA flexible composite films with enhanced energy storage density and efficiency, Compos. Sci. Technol. 151 (2017) 94-103 10.1016/j.compscitech.2017.08.013.

[16] K. Polat, Energy harvesting from a thin polymeric film based on PVDF-HFP and PMMA blend, Appl. Phys. A. 126(7) (2020) 497 10.1007/s00339-020-03698-w.

[17] X. Zhou, T. Suo, Enhanced electroactive β-phase formation in electrospun poly (vinylidene fluoride-co-hexafluoropropylene) nanowires with gold nanoparticles, Acta Mech. Sin. 38(4) (2022) 122015 10.1007/s10409-022-09036-x.

[18] D. Yuan, Z. Li, W. Thitsartarn, X. Fan, J. Sun, H. Li, C. He, β phase PVDF-hfp induced by mesoporous SiO_2 nanorods: synthesis and formation mechanism, J. Mater. Chem. C. 3(15) (2015) 3708-3713 10.1039/C5TC00005J.

[19] M. Koh, H. Hwang, D. Kim, H. Kim, Y. Hong, S.Y. Nam, Preparation and Characterization of Porous PVdF-HFP/clay Nanocomposite Membranes, Journal of Materials Science & Technology - J MATER SCI TECHNOL 26 (2010) 633-638 10.1016/S1005-0302(10)60098-9.

[20] U. Gradišar Centa, M. Sterniša, B. Višić, Ž. Federl, S.S. Možina, M. Remškar, Novel nanostructured and antimicrobial PVDF-HFP/PVP/MoO_3 composite, Surf. Innov. 9(5) (2021) 256-266 10.1680/jsuin.20.00073.

[21] M. Teodorescu, M. Bercea, Poly(vinylpyrrolidone) – A Versatile Polymer for Biomedical and Beyond Medical Applications, Polym.-Plast. Technol. Mater. 54 (2015) 923–943 10.1080/03602559.2014.979506.

[22] L.K. Mireles, M.R. Wu, N. Saadeh, L. Yahia, E. Sacher, Physicochemical Characterization of Polyvinyl Pyrrolidone: A Tale of Two Polyvinyl Pyrrolidones, ACS Omega 5(47) (2020) 30461-30467 10.1021/acsomega.0c04010.

[23] D. Heczko, B. Hachuła, P. Maksym, K. Kamiński, A. Zięba, L. Orszulak, M. Paluch, E. Kamińska, The Effect of Various Poly (N-vinylpyrrolidone) (PVP) Polymers on the Crystallization of Flutamide, Pharmaceuticals, 2022, 10.3390/ph15080971.

[24] C. Le Coz, C. Lefèbvre, F. Ludmann, E. Grosshans, Polyvinylpyrrolidone (PVP)/eicosene copolymer: An emerging cosmetic allergen, Contact dermatitis 43 (2000) 61-2.

[25] P. Franco, I. De Marco, The Use of Poly(N-vinyl pyrrolidone) in the Delivery of Drugs: A Review, Polymers (Basel) 12(5) (2020) 10.3390/polym12051114.

[26] A.I. Shawky, M.J. Megat Mohd Noor, M.M. Nasef, M. Khayet, M. Nallappan, Z. Ujang, Enhancing antimicrobial properties of poly(vinylidene fluoride)/hexafluoropropylene copolymer membrane by electron beam induced grafting of N-vinyl-2-pyrrolidone and iodine immobilization, RSC Adv. 6(48) (2016) 42461-42473 10.1039/C5RA28091E.

[27] T. Sharma, A. Joshi, A. Jain, K.R. Chaturvedi, Enhanced oil recovery and CO_2 sequestration potential of Bi-polymer polyvinylpyrrolidone-polyvinyl alcohol, J. Pet. Sci. Eng. 211 (2022) 110167 10.1016/j.petrol.2022.110167.

[28] J. Žigon, U.G. Centa, M. Remškar, M. Humar, Application and characterization of a novel PVDF-HFP/PVP polymer composite with MoO_3 nanowires as a protective coating for wood, Sci. Rep. 13(1) (2023) 3429 10.1038/s41598-023-30622-y.

[29] H. Li, J. Yang, D. Fang, L. Liu, J. Chen, M. Jiang, C. Xiong, Preparation and dielectric properties of silver@poly(vinyl pyrrolidone)/poly(vinylidene fluoride) composites, Micro Nano Lett. 11(11) (2016) 746-748 10.1049/mnl.2016.0300.

[30] U. Gradišar Centa, M. Mihelčič, V. Bobnar, M. Remškar, L. Slemenik Perše, The Effect of PVP on Thermal, Mechanical, and Dielectric Properties in PVDF-HFP/PVP Thin Film, Coatings, 2022, 10.3390/coatings12091241.

[31] S. Shenbagavalli, M. Muthuvinayagam, M.S. Revathy, Electrical properties of Mg^{2+} ion-conducting PEO: P(VdF-HFP) based solid blend polymer electrolytes, Polymer 256 (2022) 125242 10.1016/j.polymer.2022.125242.

[32] N.S. Jishnu, S.K. Vineeth, A. Das, N.T.M. Balakrishnan, A.P. Thomas, M.J. Jabeen Fatima, J.-H. Ahn, R. Prasanth, Electrospun PVdF and PVdF-co-HFP-Based Blend Polymer Electrolytes for Lithium Ion Batteries, in: N.T.M. Balakrishnan, R. Prasanth (Eds.), Electrospinning for Advanced Energy Storage Applications, Springer Singapore, Singapore, 2021, pp. 201-234.

[33] M. Ulaganathan, S. Rajendran, Preparation and characterizations of PVAc/P(VdF-HFP)-based polymer blend electrolytes, Ionics 16 (2010) 515-521 10.1007/s11581-009-0415-4.

[34] E.M. Abdelrazek, I.S. Elashmawi, A. El-khodary, A. Yassin, Structural, optical, thermal and electrical studies on PVA/PVP blends filled with lithium bromide, Curr. Appl. Phys. 10(2) (2010) 607-613 10.1016/j.cap.2009.08.005.

[35] H. Parangusan, D. Ponnamma, M.A.A. Al-Maadeed, Stretchable Electrospun PVDF-HFP/Co-ZnO Nanofibers as Piezoelectric Nanogenerators, Sci. Rep. 8(1) (2018) 754 10.1038/s41598-017-19082-3.

[36] N. Angulakshmi, S. Thomas, K.S. Nahm, A.M. Stephan, R.N. Elizabeth, Electrochemical and mechanical properties of nanochitin-incorporated PVDF-HFP-based polymer electrolytes for lithium batteries, Ionics 17(5) (2011) 407-414 10.1007/s11581-010-0517-z.

[37] D. Baganizi, E. Nyairo, S. Duncan, S. Singh, V. Dennis, Interleukin-10 Conjugation to Carboxylated PVP-Coated Silver Nanoparticles for Improved Stability and Therapeutic Efficacy, Nanomater. 7 (2017) 10.3390/nano7070165.

[38] A. Yassin, Influence of $NiCl_2$/$CdCl_2$ as Mixed Filler on Structural, Thermal and Electrical Properties of PVA/PVP Blend, Br. J. Appl. Sci. Technol. 4 (2014) 4263-4279 10.9734/BJAST/2014/12317.

[39] H.M. Zidan, E.M. Abdelrazek, A.M. Abdelghany, A.E. Tarabiah, Characterization and some physical studies of PVA/PVP filled with MWCNTs, J. Mater. Res. Technol. 8(1) (2019) 904-913 10.1016/j.jmrt.2018.04.023.

[40] Shalu, S.K. Chaurasia, R.K. Singh, S. Chandra, Thermal Stability, Complexing Behavior, and Ionic Transport of Polymeric Gel Membranes Based on Polymer PVdF-HFP and Ionic Liquid, [BMIM][BF_4], J. Phys. Chem. B 117(3) (2013) 897-906 10.1021/jp307694q.

[41] M. Sangeetha, A. Mallikarjun, M. Jaipal Reddy, J. Siva Kumar, FTIR Spectroscopic and DC Ionic conductivity Studies of PVDF-HFP: $LiBF_4$: EC Plasticized Polymer Electrolyte Membrane, IOP Conf. Ser. Mater. Sci. Eng. 225(1) (2017) 012049 10.1088/1757-899X/225/1/012049.

[42] L. Zhang, J. Yang, X. Wang, X. He, B. Zhao, Z.-H. Tang, Y. Guangzhi, H. Qiu, Thermal Properties of Poly(vinyl chloride-co-vinyl acetate-co-2-hydroxypropyl acrylate) (PVVH) Polymer and Its Application in ZnO Based Nanogenerators, Chinese Physics Letters - CHIN PHYS LETT 28 (2011) 10.1088/0256-307X/28/1/016501.

[43] A.W. Coats, J.P. Redfern, Kinetic Parameters from Thermogravimetric Data, Nature 201(4914) (1964) 68-69 10.1038/201068a0.

[44] C. Asgreen, M.M. Knopp, J. Skytte, K. Löbmann, Influence of the Polymer Glass Transition Temperature and Molecular Weight on Drug Amorphization Kinetics Using Ball Milling, Pharmaceutics 12(6) (2020) 10.3390/pharmaceutics12060483.

[45] I. Pleşa, P.V. Noţingher, S. Schlögl, C. Sumereder, M. Muhr, Properties of Polymer Composites Used in High-Voltage Applications, Polymers, 2016, 10.3390/polym8050173.

[46] A.Y. Yassin, A.R. Mohamed, A.M. Abdelghany, E.M. Abdelrazek, Enhancement of dielectric properties and AC electrical conductivity of nanocomposite using poly (vinyl chloride-co-vinyl acetate-co-2-hydroxypropyl acrylate) filled with graphene oxide, J. Mater. Sci.: Mater. Electron. 29(18) (2018) 15931-15945 10.1007/s10854-018-9679-7.

[47] S. Sharma, M. Hasan, K.V. Rajulapati, R. Kumar, P.M. Ajayan, R.M. Yadav, Investigations on dielectric and mechanical properties of poly(vinylidene fluoride-hexafluoropropylene) (PVDF-HFP)/single-walled carbon nanotube composites, J. Nanoparticle Res. 25(12) (2023) 246 10.1007/s11051-023-05886-0.

[48] T.T.N. Vu, G. Teyssedre, S.L. Roy, C. Laurent, Maxwell–Wagner Effect in Multi-Layered Dielectrics: Interfacial Charge Measurement and Modelling, Technologies, 2017, 10.3390/technologies5020027.

[49] P. Xu, X. Zhang, Investigation of MWS polarization and dc conductivity in polyamide 610 using dielectric relaxation spectroscopy, Eur. Polym. J. 47(5) (2011) 1031-1038 10.1016/j.eurpolymj.2011.02.016.

[50] E. Passaglia, Mechanical and dielectric relaxation of crystalline polymers in relation to degree of crystallinity and morphology, Polym. Sci. Eng. 4(3) (1964) 169-177 10.1002/pen.760040307.

[51] K. Deshmukh, M.B. Ahamed, K.K. Sadasivuni, D. Ponnamma, M.A.-A. AlMaadeed, S.K. Khadheer Pasha, R.R. Deshmukh, K. Chidambaram, Graphene oxide reinforced poly (4-styrenesulfonic acid)/polyvinyl alcohol blend composites with enhanced dielectric properties for portable and flexible electronics, Mater. Chem. Phys. 186 (2017) 188-201 10.1016/j.matchemphys.2016.10.044.

[52] Z. Wang, R. Wei, X. Liu, Dielectric Properties of Reduced Graphene Oxide/Copper Phthalocyanine Nanocomposites Fabricated Through π–π Interaction, J. Electron. Mater. 46(1) (2017) 488-496 10.1007/s11664-016-4916-4.

[53] K. Hamad, M. Kaseem, F. Deri, Young G. Ko, Mechanical properties and compatibility of polylactic acid/polystyrene polymer blend, Mater. Lett. 164 (2016) 409-412 10.1016/j.matlet.2015.11.029.

[54] M. Hara, J.A. Sauer, Synergism in Mechanical Properties of Polymer/Polymer Blends, Polym. Rev. 38(2) (1998) 327-362 10.1080/15583729808544529.

[55] S. Dwivedi, M. Badole, K. Gangwar, S. Kumar, Relaxation processes and conduction behaviour in PVDF-TrFE and KNN-based composites, Polymer 232 (2021) 124164 10.1016/j.polymer.2021.124164.